2015

Tropical North Atlantic Subsurface Warming Events as a Fingerprint for AMOC Variability During Marine Isotope Stage 3

Andrew O. Parker

Matthew W. Schmidt
Old Dominion University, mwschmid@odu.edu

Ping Chang

Original Publication Citation

Parker, A. O., Schmidt, M. W., & Chang, P. (2015). Tropical North Atlantic subsurface warming events as a fingerprint for AMOC variability during marine isotope stage 3. *Paleoceanography, 30*(11), 1425-1436. doi:10.1002/2015pa002832

AGU PUBLICATIONS

Paleoceanography

RESEARCH ARTICLE
10.1002/2015PA002832

Key Points:
- Subsurface warming in tropical Atlantic fingerprints reduced AMOC
- Reduced AMOC characterized most DO stadials
- AMOC did not significantly weaken during Heinrich events 2 and 3

Correspondence to:
A. O. Parker,
parkerao@geos.tamu.edu

Citation:
Parker, A. O., M. W. Schmidt, and P. Chang (2015), Tropical North Atlantic subsurface warming events as a fingerprint for AMOC variability during Marine Isotope Stage 3, *Paleoceanography*, *30*, 1425–1436, doi:10.1002/2015PA002832.

Received 11 MAY 2015
Accepted 7 OCT 2015
Accepted article online 11 OCT 2015
Published online 5 NOV 2015

Tropical North Atlantic subsurface warming events as a fingerprint for AMOC variability during Marine Isotope Stage 3

Andrew O. Parker[1], Matthew W. Schmidt[1,2], and Ping Chang[1]

[1]Department of Oceanography, Texas A&M University, College Station, Texas, USA, [2]Department of Ocean, Earth and Atmospheric Sciences, Old Dominion University, Norfolk, Virginia, USA

Abstract The role of Atlantic Meridional Overturning Circulation (AMOC) as the driver of Dansgaard-Oeschger (DO) variability that characterized Marine Isotope Stage 3 (MIS 3) has long been hypothesized. Although there is ample proxy evidence suggesting that DO events were robust features of glacial climate, there is little data supporting a link with AMOC. Recently, modeling studies and subsurface temperature reconstructions have suggested that subsurface warming across the tropical North Atlantic can be used to fingerprint a weakened AMOC during the deglacial because a reduction in the strength of the western boundary current allows warm salinity maximum water of the subtropical gyre to enter the deep tropics. To determine if AMOC variability played a role during the DO cycles of MIS 3, we present new, high-resolution Mg/Ca and $\delta^{18}O$ records spanning 24–52 kyr from the near-surface dwelling planktonic foraminifera *Globigerinoides ruber* and the lower thermocline dwelling planktonic foraminifera *Globorotalia truncatulinoides* in Southern Caribbean core VM12-107 (11.33°N, 66.63°W, 1079 m depth). Our subsurface Mg/Ca record reveals abrupt increases in Mg/Ca ratios (the largest equal to a 4°C warming) during the interstadial-stadial transition of most DO events during this period. This change is consistent with reconstructions of subsurface warming events associated with cold events across the deglacial using the same core. Additionally, our data support the conclusion reached by a recently published study from the Florida Straits that AMOC did not undergo significant reductions during Heinrich events 2 and 3. This record presents some of the first high-resolution marine sediment derived evidence for variable AMOC during MIS 3.

1. Introduction

Understanding the role of Atlantic Meridional Overturning Circulation (AMOC) in abrupt climate change during the last glacial cycle has become a fundamental topic in Paleoceanography. Evidence suggests that a reduction of AMOC during the last deglacial played an important role in two large and abrupt cooling events on the long-term warming trend following the end of the last glacial period. These two cold periods in the North Atlantic, known as Heinrich event 1 and the Younger Dryas, likely involved changes in the density of North Atlantic water due to increasing ice sheet melting [*Bond et al*., 1999; *Clark et al*., 2001; *Menviel et al*., 2011; *Ritz et al*., 2013]. Although internal feedbacks within the climate system may initiate cold stadials [*Barker et al*., 2015], the reduced surface buoyancy of North Atlantic waters due to the flux of icebergs likely slowed the rate of deep-water formation resulting in a slowdown of AMOC and reduced northward oceanic heat transport. Considerable evidence from a number of proxies including radiocarbon, nutrient tracers, and $^{231}Pa/^{230}Th$ supports the hypothesis of a reduced AMOC during these deglacial reversals [*Curry and Oppo*, 2005; *McManus et al*., 2004]. However, our understanding of the extent to which AMOC fluctuated during the glacial period across the abrupt Dansgaard-Oeschger (DO) events of Marine Isotope Stage 3 (MIS 3, 29–59 kyr) remains uncertain.

The idea that AMOC variability could be related to DO events has long been established [*Broecker et al*., 1990; *Rahmstorf*, 2002; *Timmermann et al*., 2003; *Zhang et al*., 2015], but evidence remains limited by a lack of sufficient data from marine sediment archives. High-resolution records from MIS 3 can be a challenge to find and particularly difficult to date as the limits of radiocarbon are reached at ~40 kyr, and other means of constructing absolute age models in marine sediment cores are rare. Early studies successfully linked DO-like variability in Atlantic sediments to fluctuations in AMOC with varying success. For example, *Charles et al*. [1996] produced high-resolution isotope records from benthic foraminifera in the Southern Ocean to demonstrate a clear millennial-scale pattern of change in Circumpolar Deep Water during the last

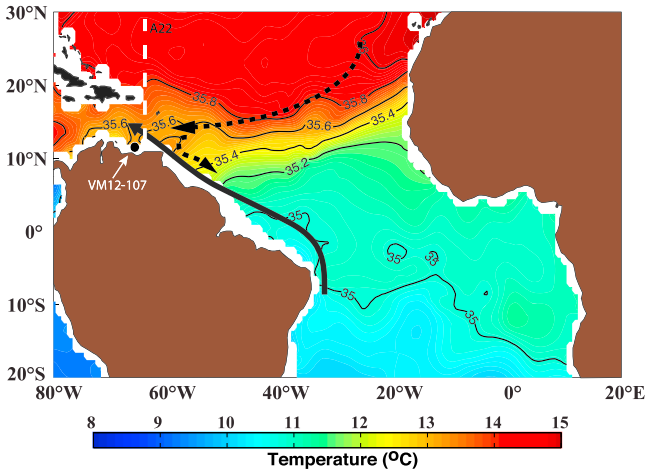

Figure 1. Modern subsurface hydrography across the Tropical Atlantic along the density surface $\sigma = 1026.8$ (~200–600 m depth). A sharp temperature (color) and salinity (contours) gradient exists in the subsurface between the subtropical gyre and the deep tropics. The warm subtropical gyre waters are blocked from flowing into the deep tropics by the northward return flow in the upper limb of the modern AMOC cell (North Brazil Current). Competition between this equatorward flow and northward AMOC return is a key element of the subsurface warming mechanism. White dashed line is cross section from World Ocean Circulation Experiment (WOCE) line A22 in Figure 2.

glacial. This observation was later confirmed in the same core by *Piotrowski et al*. [2005] using Nd isotopes to track changes in northern versus southern source waters in the Southern Ocean during MIS 3 and the last deglacial. Furthermore, *Keigwin and Boyle* [1999] measured δ^{13}C values of benthic foraminifera from a deep sediment core on the Bermuda Rise and found comparable changes in deep water formation during MIS 3. Using similar methods, *Elliot et al*. [2002] also showed changes in benthic foraminiferal δ^{13}C values corresponding to DO stadials, and *Vautravers et al*. [2004] found millennial-scale variability of deep water δ^{13}C from the Blake Ridge, albeit only during some DO stadials. Other methods including sediment magnetic susceptibility and trace metals have also traced DO-like variability in Atlantic sediments to deep ocean circulation. A benthic foraminiferal Mg/Ca record from the Iberian Margin published by *Skinner and Elderfield* [2007] showed a correlation between deep water temperature change and Greenland climate during MIS 3. Recently, this warming has been hypothesized to have played a key role in ice sheet destabilization during MIS 3, allowing for minor perturbations arising from sea ice-ice sheet-ocean interactions to significantly affect AMOC [*Alvarez-Solas et al*., 2013; *Dokken et al*., 2013; *Marcott et al*., 2011]. Furthermore, few proxies have the ability to directly monitor changes in AMOC strength. Kinematic proxies like sediment ^{231}Pa/^{230}Th ratios track the export of ^{231}Pa relative to ^{230}Th from the Atlantic as a proxy for deep water export [*McManus et al*., 2004], and nutrient proxies such as Cd/Ca, and δ^{13}C measured in benthic foraminifera can be used to reconstruct changes in Atlantic water mass geometry associated with differing AMOC states [*Curry and Oppo*, 2005]. Yet in spite of these recent advances, there is still only limited paleoceanographic evidence supporting a relationship between DO events and AMOC variability [*Clement and Peterson*, 2008].

In this study, we reconstruct past subsurface temperature changes in the western boundary current in the Tropical North Atlantic (TNA) as a new proxy for AMOC variability during MIS 3. *Zhang* [2007] established the relationship between TNA subsurface warming and AMOC weakening based on water hosing experiments and then used observed TNA subsurface anomalies to infer AMOC variations over the last several decades. *Chang et al*. [2008] and *Schmidt et al*. [2012b] extended the investigation of the subsurface temperature response to AMOC changes by including the equatorial and south tropical Atlantic and identified a two-step ocean teleconnection mechanism linking the subsurface warming to a weakening in AMOC. The first step of the process primarily involves oceanic adjustment in response to the AMOC change, which causes a rapid weakening in the western boundary current, resulting in a subsurface warming in the TNA by reducing the transport of the cold and fresh subsurface tropical water into the Caribbean region. The second step of the process becomes effective when AMOC weakens beyond a threshold, at which point the equatorward pathway of the North Atlantic subtropical cell opens, allowing the warm salinity maximum waters (SMW) of the subtropical North Atlantic gyre to flow south and warm the subsurface of the equatorial zone. This causes a warming of the equatorial and south tropical Atlantic. Today, the warm salinity maximum waters of the subtropical North Atlantic gyre remain separated from the cooler, fresher tropical subsurface waters because the equatorward pathway of the North Atlantic subtropical cell is blocked by the strong northward return flow of AMOC along the western boundary (Figure 1) [*Fratantoni et al*., 2000; *Hazeleger and Drijfhout*, 2006;

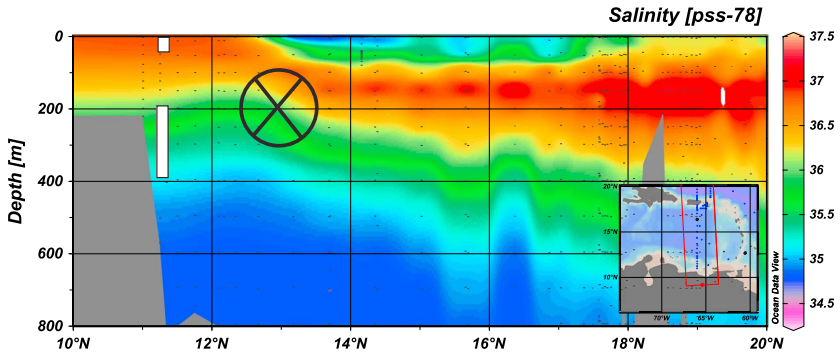

Figure 2. Vertical cross section across the Caribbean showing mean annual salinity along WOCE line A22 between 0 and 800 m. Salinity Maximum Waters are clearly defined as a salinity max at ~200 m. Subsurface conditions at the Bonaire Basin (11.33°N) are considerably fresher as the western boundary current flows just north of the basin (black circle with the X). White boxes at the core site correspond to the depth habitats of *G. ruber* (surface) and *G. truncatulinoides* (subsurface). *G. truncatulinoides* is well positioned to record changes in water masses as a result of western boundary current weakening. Figure made with Ocean Data View4.

Jochum and Malanotte-Rizzoli, 2001; *Kirchner et al*., 2009]. Modeling results in *Schmidt et al*. [2012b] showed that a major reduction in AMOC under Last Glacial Maximum (LGM) forcings and boundary conditions can produce a strong subsurface warming in the western TNA and equatorial Atlantic, providing evidence this mechanism could have operated under glacial conditions. *Schmidt et al*. [2012b] also analyzed Mg/Ca ratios in the subthermocline dwelling planktonic foraminifera *Globorotalia crassaformis* in core VM12-107 from the Southern Caribbean to reconstruct a record of deglacial subsurface temperature change (see Figure 1 for core location). Their results showed significant subsurface warming at the start of the Younger Dryas and Heinrich event 1 that covaried with changes in AMOC variability across the deglacial, demonstrating a link between AMOC weakening and subsurface warming in the TNA, likely through the first step of the proposed mechanism.

Here we extend the record from core VM12-107 (11.33°N, 66.63°W, 1079m) from the Bonaire Basin in the Southern Caribbean to reconstruct high-resolution (90 year/sample) records of surface and subsurface temperature and $\delta^{18}O_{seawater}$ ($\delta^{18}O_{sw}$, a proxy for salinity) to determine if similar subsurface temperature variability is observed during the DO events of MIS 2 and 3 (22–52 kyr). We use the upper mixed layer planktonic foraminifera *Globigerinoides ruber* to reconstruct near-surface conditions and the subthermocline dwelling planktonic foraminifera *Globorotalia truncatulinoides* to reconstruct temperature at intermediate depths (~200–400 m depth range). Our results show subsurface warming accompanies the transition from interstadial to stadial conditions during most DO events across this interval, suggesting AMOC did weaken during DO stadials.

2. Oceanographic Setting

VM12-107 is located in the Bonaire Basin, just northwest of the Cariaco Basin in the Southern Caribbean Sea. The site lies in a region of seasonal coastal upwelling initiated by the seasonal migration of the Intertropical Convergence Zone (ITCZ) from 15°N to 5°S [*Haug et al*., 2001]. The mean annual SST at our site is 26.7°C. During January–March when the ITCZ is at its southernmost position, the Northeast trade winds initiate a strong coastal upwelling cell, resulting in cooler SSTs of ~25.5°C [*Antonov et al*., 2010]. SSTs peak from June–September, reaching 27.2°C as the ITCZ migrates to just north of the Bonaire Basin. In this region, the ITCZ is the primary control of seasonal rainfalls; thus, when the ITCZ is at its southernmost position during boreal winter, salinity peaks to ~36.7 and decreases to ~36.3 during summer when the ITCZ is located at its northernmost position [*Antonov et al*., 2010; *Haug et al*., 2001; *Peterson et al*., 2000].

In the subsurface, the SMW of the Caribbean are separated from the cooler and fresher subsurface waters of the Bonaire Basin. The SMW can be defined as a water mass in the open Caribbean centered between 150 and 300 m with an annual temperature and salinity of 18°C and 36.5, respectively (Figure 2). In contrast, the modern annual subsurface conditions in the Bonaire Basin range from 19°C at 150 m to 13°C at 300 m and salinities of 36 and 35.5, respectively [*Antonov et al*., 2010]. As these SMW are presently deflected away

Table 1. VM12-107 Raw AMS ^{14}C Ages and Calibrated Calendar Ages Using the Calib 7.1 Program and a Standard Marine Reservoir Age Correction of 400 Years[a]

Depth (cm)	14C Age	Age Error (y)	Calendar Age (kyr)	(−) Error (kyr)	(+) Error (kyr)
2.5	1140	35	0.69	0.05	0.07
70.5	7900	55	8.37	0.13	0.13
82.5	9380	40	10.22	0.07	0.12
90.5	10050	65	11.05	0.26	0.14
104.5	10400	50	11.46	0.22	0.23
130.5	11200	50	12.67	0.1	0.16
160.5	12750	50	14.37	0.35	0.52
180.5	13450	60	15.74	0.56	0.64
220.5	15600	60	18.47	0.42	0.18
270.5	18500	90	21.59	0.26	0.47
318.5	19500	160	23.00	0.23	0.23
388.5	22300	220	26.14	0.23	0.2
416.5	23500	260	27.37	0.19	0.23
446.5	**26000**	**360**	**29.77**	**0.45**	**0.49**
466.5	25300	320	28.95	0.33	0.35
506.5	28400	470	31.96	0.62	0.47
548.5	29400	450	33.06	0.46	0.63
601.5	32200	170	35.69	0.21	0.23
688.5	35000	930	39.02	2.34	2.05

[a]The age in bold reflects that age reversal which was omitted from our age model.

from our site due to the strong western boundary current flowing through the Caribbean (Figure 2), several deep water channels (up to 1500 m) allow water in Bonaire Basin to freely exchange with the open Caribbean, and therefore, intermediate depth water changes in the western boundary current will affect hydrographic conditions in the basin.

To reconstruct surface conditions, we use the near-surface dwelling planktonic foraminifera *G. ruber* (white). *G. ruber* lives between 0 and 30 m depth and does not migrate to deeper waters to add a layer of gametogenic calcite at the end of its life cycle [*Bé*, 1980], so it is ideal for reconstructing tropical surface water conditions of the past [*Elderfield and Ganssen*, 2000; *Lea et al*., 2000, 2002]. Subsurface proxy records are generated using the deeper-dwelling planktonic foraminifera *G. truncatulinoides* (right coiling). Numerous studies from the Caribbean assign *G. truncatulinoides* a modern depth habitat of 200–400 m, ideally within the SMW depth range in the open Caribbean (Figure 2) [*Cleroux et al*., 2009; *Steph et al*., 2009]. Despite the tendency for *G. truncatulinoides* to have large vertical migrations within the water column, Mg/Ca and $\delta^{18}O_{calcite}$ ($\delta^{18}O_c$) values suggest calcification occurs in the lower thermocline in the tropical Atlantic [*Anand et al*., 2003; *Cleroux et al*., 2008; *McKenna and Prell*, 2004; *Sadekov et al*., 2009]. Although *Cleroux et al.* [2009] found evidence that *G. truncatulinoides* may have migrated to a shallower depth range during the last deglacial in the Florida Straits, they hypothesized that this was the result of increased continental runoff and increased turbidity in the Florida Straits, forcing *G. truncatulinoides* to shallower depths for feeding [*Cleroux et al*., 2009]. Because the Bonaire Basin would have remained far south of any significant deglacial or MIS 2 and 3 meltwater runoff, it likely did not experience similar changes in salinity and turbidity. Therefore, it is less likely that the depth habitat of *G. truncatulinoides* underwent significant changes in the past at the Bonaire Basin.

3. Materials and Methods

3.1. Age Model Development

The MIS 2 and 3 age model for VM12-107 is based on nine monospecific planktonic foraminifera (*G. ruber*) samples analyzed for radiocarbon dates at the National Ocean Sciences Accelerator Mass Spectrometer facility at Woods Hole Oceanographic Institution. Radiocarbon ages were then converted to calendar ages using CALIB 7.1 using a standard marine reservoir age correction of 400 years (Table 1). Despite recent evidence from the Cariaco Basin suggesting this reservoir age may have varied by several hundred years during periods of AMOC slowdown during the deglacial [*Muscheler et al*., 2008; *Southon et al*., 2012], it is likely that these large changes were limited to localized areas such as the Cariaco Basin and did not affect the open Caribbean/Atlantic to a similar degree [*Southon et al*., 2012].

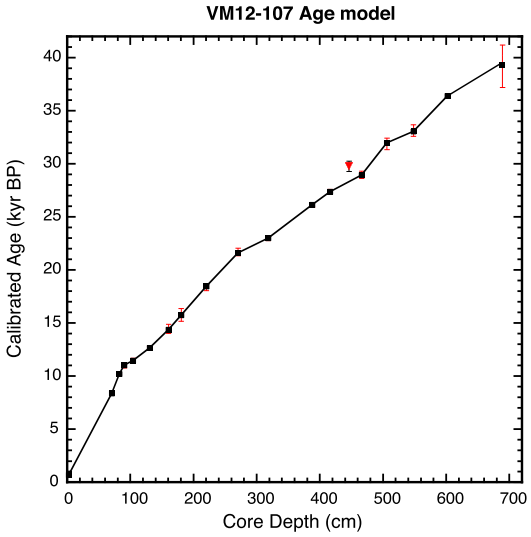

Figure 3. The MIS 2 and 3 age model for VM12-107 is based on nine calibrated radiocarbon dates between 300 and 688 cm on the planktonic foraminifera *G. ruber*, in addition to 10 previously published radiocarbon dates spanning the deglacial interval [*Schmidt et al.*, 2012b]. The resulting sedimentation rate based on linear interpolation was 22 cm/kyr. One out of sequence date at 446.5 cm was omitted from the age model (red triangle).

Each radiocarbon date was converted to the most probable calendar age, and plotted on Figure 3 with red error bars representing the 2 sigma error on the calibrated calendar age. Using linear interpolation between dates, our age model indicates a near-constant MIS 2 and 3 sedimentation rate of 22 cm/kyr (Figure 3). This is very similar to the previously published deglacial age model (sedimentation rate of 18 cm/kyr) based on 10 calibrated ^{14}C dates from the deglacial and Holocene [*Schmidt et al.*, 2012b]. Although an age reversal in our radiocarbon dates occurs between the dates at 446.5 cm and 466.5 cm (Figure 3), the date for the 446.5 cm interval falls on a radiocarbon plateau, resulting in a large calibrated age range of more than ±450 years (Table 1). Given the smaller age range for the calibrated date for the 466.5 cm interval and the visually out of sequence placement of the date at 446.5 cm (Figure 3), we decided to omit the radiocarbon date at 446.5 cm from our age model. However, it is important to note that inclusion of the date at 446.5 cm does not significantly alter our age model or change the interpretation of our results. Beyond the final ^{14}C date at 39 kyr (689 cm core depth), we did not have a straightforward means to confidently assign ages for the final 120 cm of our record. We tried correlating the *G. ruber* $\delta^{18}O$ and Mg/Ca-SST records to North Greenland Ice Core Project (NGRIP) but did not find a consistent relationship. This could be due, in part, to minor drying and cracking in this section of core that was noted during the collection of our samples by the technician at Lamont Doherty Earth Observatory. Therefore, to estimate ages in the last 120 cm of our core samples, we linearly extrapolated our MIS 2 and 3 average sedimentation rate. However, as a result of the uncertainties in dating this part of our record, we focus our interpretation and conclusions on the radiocarbon-constrained portion of our record ending at ~41 kyr.

3.2. Stable Isotope Analysis

The core was sampled at 2 cm resolution from 300 to 890 cm, corresponding to a MIS 2 and 3 temporal resolution of ~90 years/sample. First, sediment samples were disaggregated in ultraclean water for 4 h on a shaker table and then wet sieved using a 63 μm mesh. In order to limit ontogenetic and growth rate effects and to ensure an average population value, 15–20 *G. ruber* specimens were picked from the 250–355 μm size fraction for each $\delta^{18}O$ measurement. Samples were then sonicated for 5–10 s in methanol and analyzed whole on a Thermo Scientific MAT 253 IR-MS with Automated Kiel IV Carbonate Device at the Texas A&M College of Geoscience Stable Isotope Facility. The raw $\delta^{18}O$ values were standardized using NBS-19 and the long-term analytical precision on standards was less than ±0.07‰.

3.3. Trace Metal Analysis

Trace metal analyses were performed on ~580 μg of *G. ruber* (35–40 shells, 250–355 μm size range) and *G. truncatulinoides* (7–10 shells, 355–425 μm size range) from each sample. Size fractions where chosen based on the shell sizes used in the Mg/Ca temperature calibration equations (see section 3.4) and depth of habitat [*Steph et al.*, 2009]. Foraminifera were gently crushed between two glass slides, homogenized, and then split into aliquots for duplicate analyses. We followed the cleaning procedure of *Schmidt et al.* [2012a], which includes sonication in ultrapure water and methanol to remove clays, a hot water bath in reducing agents to remove metal oxides and a final hot water bath in oxidizing agents to remove organic material. Samples were then transferred into new, acid-leached vials and leached with weak nitric acid.

Finally, samples were analyzed in replicate on a Thermo Scientific Element XR High Resolution Inductively Coupled Plasma Mass Spectrometer at Texas A&M using isotope dilution. Based on a synthetic, matrix-matched Mg/Ca standard analyzed throughout this study, the analytical reproducibility for Mg/Ca was 1.20%. The pooled standard deviation on *G. ruber* duplicates is ± 4.0% (df = 272) based on 285 intervals, and on *G. truncatulinoides* duplicates is ± 4.3% (df = 203) based on 230 intervals. All data are archived at the NOAA National Climate Data Center (http://www.ncdc.noaa.gov/paleo/paleo.html).

3.4. Calibration Equations

Measurements of Mg/Ca ratios in planktonic foraminiferal shells are a widely used tool for reconstructing past ocean temperatures [*Koutavas and Lynch-Stieglitz*, 2003; *Lea et al*., 2000; *Rosenthal et al*., 2003]. Both culturing studies [*Honisch et al*., 2013; *Lea*, 1999; *Mashiotta et al*., 1999; *Russell et al*., 2004] as well as sediment and core top studies [*Anand et al*., 2003; *Dekens et al*., 2002; *Elderfield and Ganssen*, 2000; *Hastings et al*., 1998; *McConnell and Thunell*, 2005; *McKenna and Prell*, 2004; *Rosenthal et al*., 1997] show that temperature is the primary control of Mg/Ca ratios in formainiferal calcite. Although one study of core top sediments across an Atlantic meridional transect claimed that salinity had a much stronger control on foraminiferal Mg/Ca ratios than temperature [*Arbuszewski et al*., 2010], a new study showed that this conclusion likely resulted from latitudinal differences in foraminiferal dissolution resulting from regional productivity variability in surface waters and the incorrect application of a single depth-corrected Mg/Ca: SST calibration across the entire Atlantic basin [*Hertzberg and Schmidt*, 2013]. *Regenberg et al*. [2014] recently confirmed the fact that it is critically important to consider the heterogeneous effects of dissolution across the Atlantic (even at a single depth horizon) when generating Mg/Ca-SST records, and endorsed the conclusions drawn by *Hertzberg and Schmidt* [2013].

Given the shallow depth of VM12-107 and the well-preserved nature of foraminiferal tests in the core, we chose the following Mg/Ca: temperature calibrations of *Anand et al*. [2003] to reconstruct surface and subsurface temperature changes using *G. ruber* and *G. truncatulinoides*, respectively:

1. Multiplanktonic foraminifera calibration: $Mg/Ca = 0.38 \exp(0.09 \times T)$ (error ± 1.1°C),
2. *G. truncatulinoides* $Mg/Ca = 0.359 \exp(0.09 \times T)$ (error ± 1.1°C).

We chose to use the species specific Mg/Ca: temperature equation for *G. truncatulinoides* because it calculates a modern temperature of 14.2°C, a good match with this species' modern depth habitat in the Bonaire Basin (Figure 2).

The oxygen isotopic composition of foraminiferal calcite is a function of both temperature and the isotopic composition of seawater ($\delta^{18}O_{sw}$) in which an individual shell precipitates. Because $\delta^{18}O_{sw}$ covaries linearly with salinity [*Charles and Fairbanks*, 1990], shell $\delta^{18}O_c$ can be used to estimate past salinity change if the temperature component can be isolated. Therefore, researchers developed a multiproxy geochemical approach for calculating past changes in $\delta^{18}O_{sw}$ based on Mg/Ca paleothermometry and $\delta^{18}O_c$ measurements [*Carlson et al*., 2008; *Lea et al*., 2000; *Schmidt and Lynch-Stieglitz*, 2011; *Schmidt et al*., 2012a; *Weldeab et al*., 2007]. Numerous studies have used the low-light temperature: $\delta^{18}O$ relationship of *Bemis et al*. [1998] determined in laboratory culture experiments on the planktonic foraminifera *Orbulina universa* to compute $\delta^{18}O_{sw}$ in the Caribbean [*Lea et al*., 2000; *Schmidt et al*., 2004]. We also use the relationship from *Bemis et al*. [1998] to calculate $\delta^{18}O_{sw}$ using *G. ruber* $\delta^{18}O_c$ and Mg/Ca derived SST.

3. $T(°C) = 16.5 - 4.80\ (\delta^{18}O_c - (\delta^{18}O_{sw} - 0.27‰))$ (error ± 0.7°C).

4. Results

4.1. *G. ruber* $\delta^{18}O_c$

The *G. ruber* $\delta^{18}O_c$ shows a long-term enrichment of nearly 0.8‰ from 50 to 22 kyr which reflects the progressive global cooling and build up of continental ice volume leading up to the LGM around 21 kyr (Figure 4a). Overlain on the long-term trend, the *G. ruber* $\delta^{18}O_c$ record displays numerous millennial-scale events, the largest of which increases by 0.6‰ within three samples (or about 300 years) at the onset of the stadial after DO 8 (37 kyr). Abrupt increases in $\delta^{18}O_c$ are also seen for stadials after DO 5, 7, and 11. Because foraminiferal $\delta^{18}O_c$ values reflect both temperature and salinity, these positive excursions in the $\delta^{18}O_c$ record suggest either significant cooling and/or increased salinity of surface waters in the Bonaire Basin during stadials.

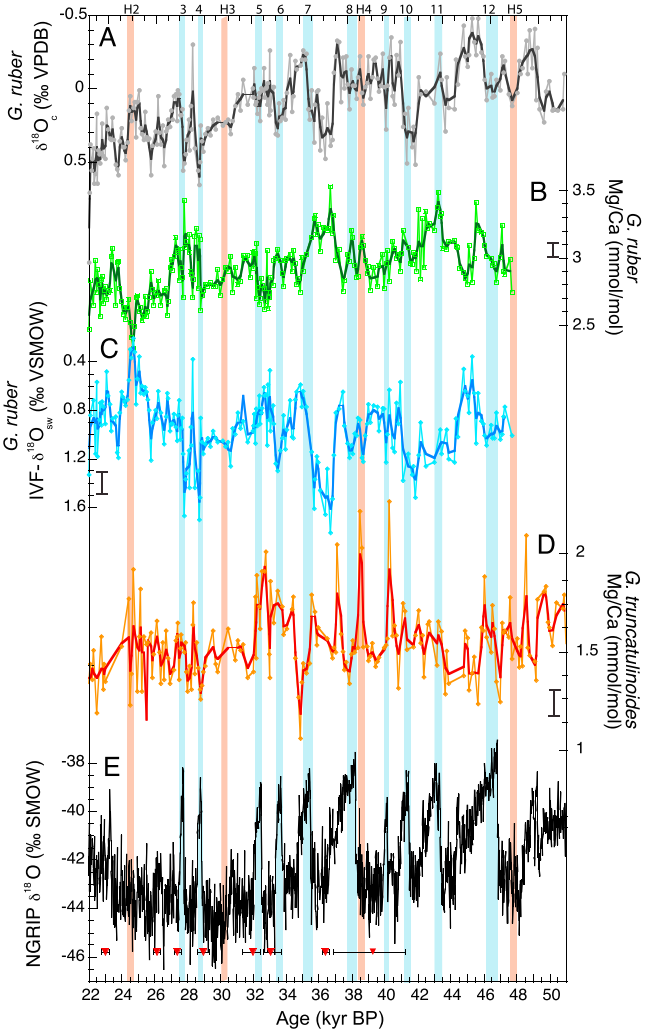

Figure 4. *G. ruber* and *G. truncatulinoides* stable isotope and trace metal data. (a) *G. ruber* $\delta^{18}O_c$ (grey line: data; black line: 3pt weighted mean), (b) *G. ruber* Mg/Ca (light green line: data; dark green line: weighted 3pt mean) and 1 sigma error next to axis, (c) *G. ruber* IVF-$\delta^{18}O_{sw}$ (light blue: data; dark blue: weighted 3pt mean) and 1 sigma error next to axis, (d) *G. truncatulinoides* Mg/Ca (orange line: data; red line: weighted 3pt mean) and 1 sigma error next to axis, (e) NGRIP $\delta^{18}O$ ice core record. Progressive cooling of glacial climate is seen in the $\delta^{18}O_c$ and Mg/Ca records as well as progressive freshening in the IVF-$\delta^{18}O_{sw}$. Superimposed on this trend are numerous millennial scale events that correlate with DO events in Greenland. Light blue boxes highlight peak interstadial conditions for each DO event. Orange boxes denote Heinrich events.

4.2. *G. ruber* Mg/Ca

G. ruber Mg/Ca ratios during MIS 2 and 3 range from 2.4 to 3.4 mmol/mol, with an average value of 2.92 mmol/mol. A correlation coefficient of −0.08 between shell weights and *G. ruber* Mg/Ca ratios provides evidence that dissolution did not significantly alter original Mg content. Overall, the *G. ruber* Mg/Ca record also shows a long-term decreasing trend of nearly 0.4 mmol/mol, equivalent to ~1.5°C, supporting the observation from $\delta^{18}O_c$ of progressive cooling leading up to the LGM (Figure 4b). Superimposed on the long-term cooling seen in the *G. ruber* Mg/Ca record are rapid increases in Mg/Ca ratios as large as 0.8 mmol/mol at DO 4, 5, 6, 8, 11, and 12. This equates to a change in temperature of ~3°C using (1). Abrupt increases in SST are mostly associated with interstadials in the Greenland stable oxygen isotope record (Figure 4e). To explore this relationship, we calculated correlation coefficients between our *G. ruber* Mg/Ca record and NGRIP ice core $\delta^{18}O$ record for the section of the core constrained by radiocarbon dates (22–41 kyr) and for the section of the core possibly affected by shrinkage (42–48 kyr). An overall positive correlation of $r = 0.24$ was found for the period between 22 and 41 kyr. In contrast, we calculate a correlation of only $r = 0.06$ for the period from 42 to 48 kyr. This supports our earlier assumption that the final 6 kyr of the core was likely compromised by drying and cracking during storage. Therefore, we limit our interpretation to the section of the core containing radiocarbon dates and not affected by core desiccation.

4.3. *G. ruber* $\delta^{18}O_{sw}$

Next, we calculate $\delta^{18}O_{sw}$ by combining the *G. ruber* Mg/Ca derived SST and the measured $\delta^{18}O_c$ using (3). We then corrected for continental ice volume change during this period using the sea-level record from *Waelbroeck et al.* [2002] to calculate the ice-volume free (IVF)-$\delta^{18}O_{sw}$ record (Figure 4c). Average MIS 2 and 3 IVF-$\delta^{18}O_{sw}$ was 0.93‰ and remained more positive (saltier) than the modern IVF-$\delta^{18}O_{sw}$ values of 0.20‰. The most positive values in our record occur during H2. The largest oscillation is associated with the stadial after DO 8, suggesting a 0.9‰ increase in IVF-$\delta^{18}O_{sw}$ values at about 37.5 kyr. In addition, the stadials after DO 5 and 7 record similar magnitude increases in IVF-$\delta^{18}O_{sw}$ as large as 0.7‰. Nevertheless, there is no significant correlation between our IVF-$\delta^{18}O_{sw}$ record and the NGRIP $\delta^{18}O$ record (correlation coefficient of −0.08).

4.4. *G. truncatulinoides* Mg/Ca Temperatures

Between 24 and 48 kyr, Mg/Ca ratios in *G. truncatulinoides* range from 2.2 to 1.1 mmol/mol with an average value of 1.55 mmol/mol. The low correlation of −0.05 between *G. truncatulinoides* shell weights and Mg/Ca ratios rules out the possibility of a significant influence of dissolution on the *G. truncatulinoides* Mg/Ca record. A ~0.2 mmol/mol decrease characterizes the long-term variability of this record through MIS 2 and 3, consistent with the stable isotope data from *G. ruber*, indicating a prolonged cooling leading up the LGM. Superimposed on this gradual decrease are abrupt increases in Mg/Ca (~0.6. mmol/mol) at the onset of stadial conditions after DO 4, 6, 7, 8, and 10, as well as during H4 (Figure 4). The average increase in Mg/Ca ratios across these events is about 0.43 mmol/mol. Using calibration (2), this equates to a warming of ~3.5°C during most of these subsurface warming events. In general, these warm pulses occur at the initial onset of stadial conditions and appear to be a robust feature in five of the eight DO interstadial-transitions that are within the radiocarbon constrained portion of our record back to about 41 kyr (DO 4, 6, 7, 8, 10, and H4). However, the two stadials following DO 3 and 9 are not associated with subsurface warming events. Nevertheless, these are particularly short DO events in the Greenland oxygen isotope record, and it is therefore possible that either the change in AMOC was too weak or our record may not have the resolution to resolve the subsurface warming associated with these brief events. It is also interesting to note that the subsurface warming does not appear to be sustained for the duration of the entire stadial event but rather appears as a brief pulse at the onset of stadial conditions that lasts only a few hundred years. In addition, there is no increase in Mg/Ca at Heinrich events 2 and 3.

5. Discussion

Our *G. ruber* stable isotope and trace metal data show clear, millennial-scale variability during MIS 2 and 3. If both *G. ruber* and *G. truncatulinoides* were recording hydrographic conditions reflecting the propagation of SMW into the Bonaire Basin, we might expect that the *G. ruber* data would record an increase in salinity and temperature when the *G. truncatulinoides* warm. Indeed, this is the case during the stadial between DO 7 and 8 (36–38.5 kyr, 610–650 cm) when the two records broadly support the presence of SMW in the Bonaire Basin with a correlation between *G. ruber* IVF-$\delta^{18}O_{sw}$ and *G. truncatulinoides* Mg/Ca equal to −0.77. However, this appears to be the only time where the two species are definitively recording similar conditions. Although the *G. truncatulinoides* Mg/Ca record suggests warming during several stadial events, the *G. ruber* data are less consistent. In many cases, the *G. ruber* Mg/Ca and IVF-$\delta^{18}O_{sw}$ data show cool/fresh or warm/fresh surface conditions in the Bonaire Basin during stadial events, for example, at 29, 34.5, and 40 kyr. We suspect the inconsistency between the *G. ruber* and *G. truncatulinoides* records results from the fact that the *G. ruber* record is affected by the strong seasonality of surface waters in this region caused by the annual migration of the ITCZ [*Peterson et al*., 2000; *Haug et al*., 2001]. Today, the ITCZ sits north of the Bonaire Basin during summer, resulting in relatively warm, evaporative conditions in the basin. This seasonality is expressed in surface salinity, with 36.7 during summer and slightly lower at 36.3 during the wet winter. In addition, sea surface conditions in the Bonaire Basin are also influenced from the subsurface. During winter when the ITCZ is located south of the Bonaire Basin, the NE Trade winds cause upwelling to develop at the site (Figure 2). *Wan et al*. [2009] used a coupled ocean-atmosphere model to analyze how atmospheric and ocean circulation changes associated with a cooling of the North Atlantic affected the Southern Caribbean. In their model, they found that the enhanced evaporative cooling due to the strengthened surface wind and the advection of cooler and drier air from the north led to a surface cooling while ocean circulation changes caused a strong subsurface warming in this region. They concluded that this region is influenced by contrasting atmospheric changes from above and ocean circulation changes from below the sea surface during cold periods in the North Atlantic. Therefore, it is likely that the Bonaire Basin *G. ruber* records integrate both oceanic and atmospheric signals, making them difficult to interpret, especially during periods of enhanced upwelling. We believe that is why it is difficult to identify a strong phase relationship between our *G. ruber* records and the Greenland ice core $\delta^{18}O$ record.

As discussed in *Zhang* [2007], *Chang et al*. [2008] and *Schmidt et al*. [2012b], a major reduction of AMOC can cause a significant weakening in the western boundary current through primarily oceanic wave adjustment, i.e., the first step of the process of the ocean teleconnection mechanism by *Chang et al*. [2008] and *Schmidt et al*. [2012b]. This results in strong subsurface warming in the western boundary current in the Southern Caribbean and in the western tropical Atlantic. Warming pulses observed in our *G. truncatulinoides* Mg/Ca

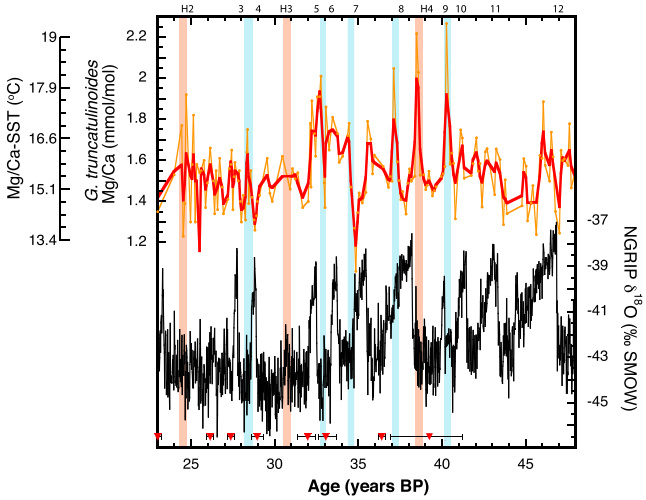

Figure 5. *G. truncatulinoides* Mg/Ca data (orange line: data; red line: weighted 3 point mean) and NGRIP $\delta^{18}O$ ice core record (black line) for comparison. Light blue boxes represent DO intervals with apparent subsurface warming and are centered on the warming event. Orange boxes represent Heinrich events. Abrupt warmings of ~0.6 mmol/mol or ~3.5°C characterize the onset of most DO stadials. Note that subsurface warming events are not associated with Heinrich events 2 and 3; however, a large subsurface warming occurs at Heinrich event 4, possibly indicating Heinrich 2 and 3 were not associated with AMOC weakening.

record are consistent with this mechanism during most DO cycles. Within the timespan of our reconstructions, we find evidence for subsurface warming during the stadials after DO 4, 6, 7, 8, and 10, as well as during H4 (Figure 5). The pulse-like nature of these warmings also suggests that the second step of the process of the ocean teleconnection mechanism plays an important role for the termination of the events. As the AMOC continues to weaken, the equatorward pathway of the North Atlantic subtropical cell begins to open, allowing the warm SMW to escape the Southern Caribbean Sea, terminating the TNA subsurface warming and eventually replacing the warm water by cooler water [*Chang et al*., 2008]. Therefore, rather than a sustained warming for the duration of the stadial, cooler waters quickly follow the initial warming pulse. Interstadials are characterized by cooler subsurface conditions as AMOC strength increases and allows for the establishment of the steep subsurface gradient with warmer waters in the North Atlantic gyre and cooler waters in the deep Tropics (Figure 1). DO stadials 3 and 9 do not show a subsurface warming. These DO events are relatively small, short events compared to the much larger DO 7 and 8 where robust warming is recorded. It is possible that no subsurface warming is recorded for these events because they are too short for the temporal resolution of our record to resolve. Or a second possible explanation could be that there was not a large enough slowdown of AMOC to permit SMW into the Caribbean during these stadials. In addition, there does not appear to be a relationship between the size and duration of a DO event and the magnitude of subsurface warming in the TNA; the shorter DO events 4, 6, and 10 show the same amount of subsurface warming of ~3°C in the following stadials as does the larger DO 8 at 37.5 kyr.

Although modeling results indicate subsurface temperatures in the Bonaire Basin should be sensitive to AMOC variability [*Schmidt et al*., 2012b], it is also possible that other oceanographic and atmospheric circulation changes affected the vertical temperature profile at our core site. High-resolution studies from the nearby Cariaco Basin showed that the ITCZ in the tropical Atlantic shifts south during cold periods in the North Atlantic, resulting in increased upwelling along the northern coast of South America [*Peterson et al*., 1991 and 2000]. As the ITCZ shifted southward away from the Southern Caribbean, the Bonaire Basin would have been more influenced by the Northeast Trades for longer periods of time, most likely resulting in enhanced coastal upwelling. During these times, we would expect the thermocline to shoal and the upper water column to cool. Nevertheless, during many of the DO stadials in our record, we find just the opposite: a warming of subsurface conditions at our site. Therefore, we believe subsurface changes associated with AMOC variability are the most likely driver of subsurface temperature change in the Bonaire Basin.

The observations of abrupt warmings in the *G. truncatulinoides* Mg/Ca data during the onset of stadial conditions in Greenland are also consistent with the subsurface warming observed in *Schmidt et al*. [2012b] across the last deglacial period. Using the same core and the subsurface dwelling species *G. crassaformis*, *Schmidt et al*. [2012b] identified subsurface warmings of 3°C and 1.7°C during the YD and H1, respectively. In this study, we use *G. truncatulinoides* rather than *G. crassaformis* due to the low abundance of *G. crassaformis*

deeper in the core after the LGM. However, both species share considerable overlap in their habitat depth ranges and both live in the lower thermocline [*Steph et al*., 2009], well within the 300–600 m depth over which maximum subsurface warming occurs according to models [*Chang et al*., 2008; *Schmidt et al*., 2012b; *Zhang*, 2007]. Given these similarities, our new subsurface temperature record suggests that AMOC was in a reduced state during most of the DO stadial events of late MIS 3.

A new study by *Bohm et al*. [2015] used the water mass tracers $^{231}Pa/^{230}Th$ and ε_{Nd} to characterize Atlantic water mass export over the last full glacial-interglacial cycle. They concluded that AMOC was only slightly reduced overall during MIS 3 as compared to AMOC strength during the Holocene. Our new subsurface record would suggest that this strong mode of interstadial AMOC strength during MIS 3 was periodically reduced during stadials, suggesting that AMOC played an important role in DO climate cycles. Given their study's lower sample resolution during MIS 3, we suspect they were unable to resolve the brief periods of weak AMOC during DO stadials.

Our data also support a recent reconstruction of little or no AMOC change during Heinrich events 2 and 3. *Lynch-Stieglitz et al*. [2014] reconstructed past changes in the density gradient across the Florida Straits using benthic foraminiferal $\delta^{18}O_c$ as a proxy for AMOC variability over the past 35 kyr. Based on the geostrophic method, these researchers found no evidence for a reduction in AMOC across Heinrich events 2 and 3 and reasoned that AMOC was already in a weakened state and therefore did not experience any further reduction during these events. Similarly, our new subsurface temperature records show no warming across these two Heinrich events at 24.5 and 30.2 kyr (Figure 5). In contrast, Heinrich event 4 is recorded as a very large warming just prior to DO 8 at ~39 kyr. This Heinrich 4-DO 8 sequence is the best-resolved event in our record and suggests a strong subsurface warming during Heinrich 4 within the stadial before DO 8. While the geostrophic flow reconstructions of *Lynch-Stieglitz et al*. [2014] do not extend back to H4, *Bohm et al*. [2015] also found evidence for a significant slowdown in AMOC during H4. It is important to note that we identified the age ranges for Heinrich events as recorded in the absolute dated Hulu Cave speleothem records [*Wang et al*., 2001]. Therefore, we believe our results provide additional evidence that the mechanisms responsible for Heinrich events varied under different climate states, as concluded in *Lynch-Stieglitz et al*. [2014].

The connection between subsurface warming events in the TNA and AMOC variability during MIS 3 are also consistent with the new modeling study of *Zhang et al*. [2015] who used the CCSM3 to model AMOC response to ocean temperature anomalies under MIS 3 boundary conditions. Their data suggest AMOC varied by ~9.2 sverdrup (Sv, 10^6 m^3/s) between stadial to interstadial conditions, with a net flow of ~11 Sv during stadials. Although our method cannot quantify the magnitude of AMOC change, based on the modeling experiments of *Chang et al*. [2008] and *Schmidt et al*. [2012b] for which the subsurface warming mechanism was identified, a 0.1 Sv water hosing applied to LGM boundary conditions resulted in a similar reduction of AMOC strength to ~9.5 Sv and produced a subsurface warming near our location between 2 and 3°C. These modeling results are therefore consistent with the magnitude of *G. truncatulinoides* warming observed in our record associated with most DO stadials over the last 41 kyr.

6. Conclusions

We present new stable isotope and trace metal data from surface and subsurface dwelling planktonic foraminifera to investigate the role of AMOC during DO events. Although our new surface records of temperature and salinity change are difficult to correlate to high-latitude climate change because they are influenced by both atmospheric and ocean circulation changes during MIS 2 and 3, our subsurface temperature record reveals distinct warmings at the onset of most cold DO stadials in the North Atlantic back to 41 kyr. This pattern of subsurface warming is consistent with a subsurface warming mechanism linked to reduced northward transport in the western boundary current and the influx of SMW into the deep tropics. This pattern of surface temperature change provides evidence for an anticorrelated relationship between subsurface TNA temperatures and AMOC strength during MIS 3 and suggests that AMOC was significantly reduced during DO stadials. Additionally, our results support recent conclusions reached by *Lynch-Stieglitz et al*. [2014] that glacial Heinrich events 2 and 3 saw little change in the strength of AMOC. Collectively, our new records provide insight into the dynamic processes that influenced glacial climate.

Acknowledgments
This work was supported by a National Science foundation grant to M.W.S. and P.C. (OCE-1102743). We thank Luz Romero for her technical assistance with the ICP-MS and two undergraduate lab assistants for their help with lab work. We also thank the Lamont Doherty Earth Observatory core repository for sediment core material. A.O.P. was also supported by a National Science Foundation S-STEM grant. All new data presented in this paper are readily available at the NOAA National Climate Data Center (http://www.ncdc.noaa.gov/paleo/paleo.html).

References

Alvarez-Solas, J., A. Robinson, M. Montoya, and C. Ritz (2013), Iceberg discharges of the last glacial period driven by oceanic circulation changes, *Proc. Natl. Acad. Sci. U.S.A.*, *110*(41), 16,350–16,354.

Anand, P., H. Elderfield, and M. H. Conte (2003), Calibration of Mg/Ca thermometry in planktonic foraminifera from a sediment trap time series, *Paleoceanography*, *18*(2), 1050, doi:10.1029/2002PA000846.

Antonov, J. I., D. Seidov, T. P. Boyer, R. A. Locarnini, A. V. Mishonov, and H. E. Garcia (Eds.) (2010), *World Ocean Atlas 2009*, 184 pp., U.S. Govt. Print. Off., Washington, D. C.

Arbuszewski, J., P. deMenocal, A. Kaplan, and E. Farmer (2010), On the fidelity of shell-derived δ18O seawater estimates, *Earth Planet. Sci. Lett.*, *300*, 185–196.

Barker, S., J. Chen, X. Gong, L. Jonkers, G. Knorr, and D. Thornalley (2015), Icebergs not the trigger for North Atlantic cold events, *Nature*, *520*, 333–336.

Bé, A. W. (1980), Gametogenic calcification in a spinose planktonic foraminifer, *Globigerinoides sacculifer* (Brady), *Mar. Micropaleontol.*, *5*, 283–310.

Bemis, B. E., H. J. Spero, J. Bijima, and D. W. Lea (1998), Reevaluation of the oxygen isotopic composition of planktonic foraminifera: Experimental results and revised paleotemperature equations, *Paleoceanography*, *13*(2), 150–160, doi:10.1029/98PA00070.

Bohm, E., J. Lippold, M. Gutjahr, M. Frank, P. Blaser, B. Antz, J. Fohlmeister, N. Frank, M. B. Andersen, and M. Deininger (2015), Strong and deep Atlantic meridional overturning circulation during the last glacial cycle, *Nature*, *517*(7532), 73–U170.

Bond, G., W. Showers, M. Elliot, M. Evans, R. Lotti, I. Hajdas, G. Bonani, and S. Johnson (1999), The North Atlantic's 1–2 kyr climate rhythm: Relation to Heinrich Events, Dansgaard/Oeschger Cycles and the Little Ice Age, in *Mechanisms of Global Climate Change at Millennial Timescales*, edited by P. U. Clark, R. S. Webb, and L. D. Keigwin, pp. 35–58, AGU, Washington, D. C.

Broecker, W. S., G. Bond, M. Klas, G. Bonani, and W. Wolfli (1990), A salt oscillator in the glacial Atlantic? The concept, *Paleoceanography*, *5*(4), 469–478, doi:10.1029/PA005i004p00469.

Carlson, A. E., D. W. Oppo, R. E. Came, A. N. LeGrande, L. D. Keigwin, and W. B. Curry (2008), Subtropical Atlantic salinity variability and Atlantic meridional circulation during the last deglaciation, *Geology*, *36*(12), 991–994.

Chang, P., R. Zhang, W. Hazeleger, C. Wen, X. Q. Wan, L. Ji, R. J. Haarsma, W. P. Breugem, and H. Seidel (2008), Oceanic link between abrupt changes in the North Atlantic Ocean and the African monsoon, *Nat. Geosci.*, *1*(7), 444–448.

Charles, C. D., and R. G. Fairbanks (1990), Glacial to interglacial changes in the isotopic gradients of southern ocean surface water, in *Geological History of the Polar Oceans: Arctic Versus Antarctic*, edited by U. Bleil and J. Thiede, pp. 519–538, Kluwer, Netherlands.

Charles, C. D., J. Lynch-Stieglitz, U. S. Ninnemann, and R. G. Fairbanks (1996), Climate connections between the hemisphere revealed by deep sea sediment core/ice core correlations, *Earth Planet. Sci. Lett.*, *192*, 19–27.

Clark, P. U., S. J. Marshall, G. K. C. Clarke, S. W. Hostetler, J. M. Licciardi, and J. T. Teller (2001), Freshwater forcing of abrupt climate change during the last glaciation, *Science*, *293*(5528), 283–287.

Clement, A. C., and L. C. Peterson (2008), Mechanisms of abrupt climate change of the last glacial period, *Rev. Geophys.*, *46*, RG4002, doi:10.1029/2006RG000204.

Cleroux, C., E. Cortijo, P. Anand, L. Labeyrie, F. Bassinot, N. Caillon, and J. C. Duplessy (2008), Mg/Ca and Sr/Ca ratios in planktonic foraminifera: Proxies for upper water column temperature reconstruction, *Paleoceanography*, *23*, PA3214, doi:10.1029/2007PA001505.

Cleroux, C., J. Lynch-Stieglitz, M. W. Schmidt, E. Cortijo, and J. C. Duplessy (2009), Evidence for calcification depth change of Globorotalia truncatulinoides between deglaciation and Holocene in the western Atlantic Ocean, *Mar. Micropaleontol.*, *73*(1–2), 57–61.

Curry, W. B., and D. W. Oppo (2005), Glacial water mass geometry and the distribution of delta C-13 of Sigma CO2 in the western Atlantic Ocean, *Paleoceanography*, *20*, PA1017, doi:10.1029/2004PA001021.

Dekens, P. S., D. W. Lea, D. K. Pak, and H. J. Spero (2002), Core top calibration of Mg/Ca in tropical foraminifera: Refining paleotemperature estimation, *Geochem. Geophys. Geosyst.*, *4*(6), 1022, doi:10.1029/2001GC000200.

Dokken, T. M., K. H. Nisancioglu, C. Li, D. S. Battisti, and C. Kissel (2013), Dansgaard-Oeschger cycles: Interactions between ocean and sea ice intrinsic to the Nordic seas, *Paleoceanography*, *28*, 491–502, doi:10.1002/palo.20042.

Elderfield, H., and G. Ganssen (2000), Past temperature and d^{18}O of surface ocean waters inferred from foraminiferal Mg/Ca ratios, *Nature*, *405*, 442–445.

Elliot, M., L. D. Labeyrie, and J. C. Duplessy (2002), Changes in North Atlantic deep-water formation associated with the Dansgaard-Oeschger temperature oscillations (60–10 ka), *Quat. Sci. Rev.*, *21*, 1153–1165.

Fratantoni, D. M., W. E. Johns, T. L. Townsend, and H. E. Hurlburt (2000), Low-latitude circulation and mass transport pathways in a model of the tropical Atlantic ocean, *J. Phys. Oceanogr.*, *30*(8), 1944–1966.

Hastings, D. W., A. D. Russell, and S. R. Emerson (1998), Foraminiferal magnesium in *Globigerinoides sacculifer* as a paleotemperature proxy, *Paleoceanography*, *13*(2), 161–169, doi:10.1029/97PA03147.

Haug, G. H., K. A. Hughen, D. M. Sigman, L. C. Peterson, and U. Rohl (2001), Southward migration of the intertropical convergence zone through the Holocene, *Science*, *293*(5533), 1304–1308.

Hazeleger, W., and S. Drijfhout (2006), Subtropical cells and meridional overturning circulation pathways in the tropical Atlantic, *J. Geophys. Res.*, *111*, C03013, doi:10.1029/2005JC002942.

Hertzberg, J. E., and M. W. Schmidt (2013), Refining Globigerinoides ruber Mg/Ca paleothermometry in the Atlantic Ocean, *Earth Planet. Sci. Lett.*, *383*, 123–133.

Honisch, B., K. A. Allen, D. W. Lea, H. J. Spero, S. M. Eggins, J. Arbuszewski, P. deMenocal, Y. Rosenthal, A. D. Russell, and H. Elderfield (2013), The influence of salinity on Mg/Ca in planktic foraminifers—Evidence from cultures, core-top sediments and complementary delta O-18, *Geochim. Cosmochim. Acta*, *121*, 196–213.

Jochum, M., and P. Malanotte-Rizzoli (2001), Influence of the meridional overturning circulation on tropical-subtropical pathways, *J. Phys. Oceanogr.*, *31*(5), 1313–1323.

Keigwin, L. D., and E. A. Boyle (1999), Surface and deep ocean variability in the northern Sargasso Sea during marine isotope stage 3, *Paleoceanography*, *14*(2), 164–170, doi:10.1029/1998PA900026.

Kirchner, K., M. Rhein, S. Huttl-Kabus, and C. W. Boning (2009), On the spreading of South Atlantic Water into the Northern Hemisphere, *J. Geophys. Res.*, *114*, C05019, doi:10.1029/2008JC005165.

Koutavas, A., and J. Lynch-Stieglitz (2003), Glacial-interglacial dynamics of the eastern equatorial Pacific cold tongue Intertropical Convergence Zone system reconstructed from oxygen isotope records, *Paleoceanography*, *18*(4), 1089, doi:10.1029/2003PA000894.

Lea, D. W. (1999), Trace elements in foraminiferal calcite, in *Modern Foraminifera*, edited by B. K. S. Gupta, pp. 259–277, Kluwer Acad., Great Britain.

Lea, D. W., D. K. Pak, and H. J. Spero (2000), Climate impact of late quaternary equatorial Pacific sea surface temperature variations, *Science*, *289*, 1719–1724.
Lea, D. W., P. A. Martin, D. K. Pak, and H. J. Spero (2002), Reconstructing a 350 ky history of sea level using planktonic Mg/Ca and oxygen isotope records from a Cocos Ridge core, *Quat. Sci. Rev.*, *21*, 283–293.
Lynch-Stieglitz, J., M. W. Schmidt, L. G. Henry, W. B. Curry, L. C. Skinner, S. Mulitza, R. Zhang, and P. Chang (2014), Muted change in Atlantic overturning circulation over some glacial-aged Heinrich events, *Nat. Geosci.*, *7*(2), 144–150.
Marcott, S. A., et al. (2011), Ice-shelf collapse from subsurface warming as a trigger for Heinrich events, *Proc. Natl. Acad. Sci. U.S.A.*, *108*(33), 13,415–13,419.
Mashiotta, T. A., D. W. Lea, and H. J. Spero (1999), Glacial-interglacial changes in Subantarctic sea surface temperature and d^{18}O-water using foraminiferal Mg, *Earth Planet. Sci. Lett.*, *170*, 417–432.
McConnell, M. C., and R. C. Thunell (2005), Calibration of the planktonic foraminiferal Mg/Ca paleothermometer: Sediment trap results from the Guaymas Basin, Gulf of California, *Paleoceanography*, *20*, PA2016, doi:10.1029/2004PA001077.
McKenna, V. S., and W. L. Prell (2004), Calibration of the Mg/Ca of Globorotalia truncatulinoides (R) for the reconstruction of marine temperature gradients, *Paleoceanography*, *19*, PA2006, doi:10.1029/2000PA000604.
McManus, J. F., R. Francois, J.-M. Gherardi, L. D. Keigwin, and S. Brown-Leger (2004), Collapse and rapid resumption of Atlantic meridional circulation linked to deglacial climate changes, *Nature*, *428*, 834–837.
Menviel, L., A. Timmermann, O. E. Timm, and A. Mouchet (2011), Deconstructing the Last Glacial termination: The role of millennial and orbital-scale forcings, *Quat. Sci. Rev.*, *30*(9–10), 1155–1172.
Muscheler, R., B. Kromer, S. Bjorck, A. Svensson, M. Friedrich, K. F. Kaiser, and J. Southon (2008), Tree rings and ice cores reveal C-14 calibration uncertainties during the Younger Dryas, *Nat. Geosci.*, *1*(4), 263–267.
Peterson, L. C., J. T. Overpeck, N. G. Kipp, and J. Imbrie (1991), A high-resolution Late Quaternary upwelling record from the anoxic Cariaco Basin, Venezuela, *Paleoceanography*, *6*(1), 99–119, doi:10.1029/90PA02497.
Peterson, L. C., G. H. Haug, K. A. Hughen, and U. Rohl (2000), Rapid changes in the hydrologic cycle of the Tropical Atlantic during the last Glacial, *Science*, *290*, 1947–1951.
Piotrowski, A. M., S. L. Goldstein, S. R. Hemming, and R. G. Fairbanks (2005), Temporal relationships of carbon cycling and ocean circulation at glacial boundaries, *Science*, *307*, 1933–1938.
Rahmstorf, S. (2002), Ocean circulation and climate during the past 120,000 years, *Nature*, *419*(6903), 207–214.
Regenberg, M., A. Regenberg, D. Garbe-Schonberg, and D. W. Lea (2014), Global dissolution effects on planktonic foraminiferal Mg/Ca ratios controlled by the calcite-saturation state of bottom waters, *Paleoceanography*, *27*, 127–142, doi:10.1002/2013PA002492.
Ritz, S. P., T. F. Stocker, J. O. Grimalt, L. Menviel, and A. Timmermann (2013), Estimated strength of the Atlantic overturning circulation during the last deglaciation, *Nat. Geosci.*, *6*(3), 208–212.
Rosenthal, Y., E. A. Boyle, and N. Slowey (1997), Temperature control on the incorporation of magnesium, strontium, fluorine, and cadmium into benthic foraminiferal shells from Little Bahama Bank: Prospects for thermocline paleoceanography, *Geochim. Cosmochim. Acta*, *61*(17), 3633–3643.
Rosenthal, Y., D. W. Oppo, and B. K. Linsley (2003), The amplitude and phasing of climate change during the last deglaciation in the Sulu Sea, western equatorial Pacific, *Geophys. Res. Lett.*, *30*(8), 1428, doi:10.1029/2002GL016612.
Russell, A. D., B. Honisch, H. J. Spero, and D. W. Lea (2004), Effects of seawater carbonate ion concentration and temperature on shell U, Mg, and Sr in cultured planktonic foraminifera, *Geochim. Cosmochim. Acta*, *68*(21), 4347–4361.
Sadekov, A., S. M. Eggins, P. De Deckker, U. Ninnemann, W. Kuhnt, and F. Bassinot (2009), Surface and subsurface seawater temperature reconstruction using Mg/Ca microanalysis of planktonic foraminifera *Globigerinoides ruber*, *Globigerinoides sacculifer*, and *Pulleniatina obliquiloculata*, *Paleoceanography*, *24*, PA3201, doi:10.1029/2008PA001664.
Schmidt, M. W., and J. Lynch-Stieglitz (2011), Florida Straits deglacial temperature and salinity change: Implications for tropical hydrologic cycle variability during the Younger Dryas, *Paleoceanography*, *26*, PA4205, doi:10.1029/2011PA002157.
Schmidt, M. W., H. J. Spero, and D. W. Lea (2004), Links between salinity variation in the Caribbean and North Atlantic thermohaline circulation, *Nature*, *428*, 160–163.
Schmidt, M. W., W. A. Weinlein, F. Marcantonio, and J. Lynch-Stieglitz (2012a), Solar forcing of Florida Straits surface salinity during the early Holocene, *Paleoceanography*, *27*, PA3204, doi:10.1029/2012PA002284.
Schmidt, M. W., P. Chang, J. E. Hertzberg, T. R. Them, J. Link, and B. L. Otto-Bliesner (2012b), Impact of abrupt deglacial climate change on tropical Atlantic subsurface temperatures, *Proc. Natl. Acad. Sci. U.S.A.*, *109*(36), 14,348–14,352.
Skinner, L. C., and H. Elderfield (2007), Rapid fluctuations in the deep North Atlantic heat budget during the last glacial period, *Paleoceanography*, *22*, PA1205, doi:10.1029/2006PA001338.
Southon, J., A. L. Noronha, H. Cheng, R. L. Edwards, and Y. J. Wang (2012), A high-resolution record of atmospheric C-14 based on Hulu Cave speleothem H82, *Quat. Sci. Rev.*, *33*, 32–41.
Steph, S., M. Regenberg, R. Tiedemann, S. Mulitza, and D. Nurnberg (2009), Stable isotopes of planktonic foraminifera from tropical Atlantic/Caribbean core-tops: Implications for reconstructing upper ocean stratification, *Mar. Micropaleontol.*, *71*(1–2), 1–19.
Timmermann, A., H. Gildor, M. Schulz, and E. Tziperman (2003), Coherent resonant millennial-scale climate oscillations triggered by massive meltwater pulses, *J. Clim.*, *16*(15), 2569–2585.
Vautravers, M. J., N. J. Shackleton, C. Lopez-Martinez, and J. O. Grimalt (2004), Gulf Stream variability during marine isotope stage 3, *Paleoceanography*, *19*, PA2011, doi:10.1029/2003PA000966.
Waelbroeck, C., L. D. Labeyrie, E. Michel, J. C. Duplessy, J. F. McManus, K. Lambeck, E. Balbon, and M. Labracherie (2002), Sea-level and deep water temperature changes derived from benthic foraminifera isotopic records, *Quat. Sci. Rev.*, *21*, 295–305.
Wan, X. Q., P. Chang, R. Saravanan, R. Zhang, and M. W. Schmidt (2009), On the interpretation of Caribbean paleo-temperature reconstructions during the Younger Dryas, *Geophys. Res. Lett.*, *36*, L02701, doi:10.1029/2008GL035805.
Wang, Y. J., H. Cheng, R. L. Edwards, Z. S. An, J. Y. Wu, C.-C. Shen, and J. A. Dorale (2001), A high-resolution absolute-dated late Pleistocene monsoon record from Hulu Cave, China, *Science*, *394*, 2345–2348.
Weldeab, S., D. W. Lea, R. R. Schneider, and N. Andersen (2007), Centennial scale climate instabilities in a wet early Holocene West African monsoon, *Geophys. Res. Lett.*, *34*, L24702, doi:10.1029/2007GL03.
Zhang, R. (2007), Anticorrelated multidecadal variations between surface and subsurface tropical North Atlantic, *Geophys. Res. Lett.*, *34*, L12713, doi:10.1029/2007GL030225.
Zhang, X., M. Prange, U. Merkel, and H. Schulz (2015), Spatial fingerprint and magnitude of changes in the Atlantic meridional overturning circulation during Marine Isotope Stage 3, *Geophys. Res. Lett.*, *42*, 1903–1911, doi:10.1002/2014GL063003.